Mon. Not. R. Astron. Soc. **276**, 1224–1244 (1995)

Imaging of MBG starbursts – I. Morphological analysis

Clarissa S. Barth,* Roger Coziol and Serge Demers
Département de Physique, Observatoire du Monte Mégantic, Université de Montréal, Montréal, Québec, H3C 3J7 Canada

Accepted 1995 May 12. Received 1995 April 25; in original form 1994 May 10

ABSTRACT

We present, in detail, the morphological analysis of a sample of 15 galaxies of the Montreal blue galaxy (MBG) survey, based on *BVRI* imaging. The sample consists of starburst nucleus galaxies, mostly with early-type morphologies. We fit elliptical isophotes to the images, and analyse the parameters derived from the fitting procedure, the luminosity profiles, the $B-I$ colour profiles and $B-I$ colour maps. Circumnuclear regions of star formation are identified, corresponding well to the extended Hα emission measured spectroscopically. The dimensions of these extended regions are of the order of kiloparsecs. For barred galaxies, the star formation is more concentrated than for unbarred ones, which tend to have extended starbursts. A high interaction rate for the objects studied is indicated by the frequency of dust, twisted isophotes, and a wide dispersion of colours (similar to Arp–Madore galaxies), which is not correlated with the morphological type. The observed isophotal twists in our sample are related to the presence of bars, for SBa and later types, or to geometrical decoupling, for S0 and E galaxies. The level of 'boxiness' and 'discyness' is larger than that of normal early-type galaxies, reflecting the disturbed morphology of these objects. The connection of these morphological characteristics with the observed starbursts is highly probable.

Key words: galaxies: fundamental parameters – galaxies: starburst.

1 INTRODUCTION

The MBG survey is a parallel project of the Montreal–Cambridge–Tololo (MCT) survey of southern subluminous blue stars (Demers et al. 1986). Our primary goal is to explore 7000 deg^2 of the southern hemisphere, centred on the south galactic pole, in search of new, relatively bright emission-line galaxies. Up to now, we have followed a two-step procedure: step one consists of the selection of candidates from the digitally measured MCT plates, while step two consists of the classification of the galaxies following their optical spectral characteristics. Details of our method of selection and classification can be found in Coziol et al. (1993a) and Coziol et al. (1994). We find mostly starburst galaxies, where the dominant activity is related to a relatively intense phase of star formation. The AGNs constitute only 5 per cent of our candidates, a yield somewhat lower than those for the Markarian and Kiso surveys (Mazarella & Balzano 1986; Maehara et al. 1987).

The nature of the MBGs is very similar to the sampling of Markarian starburst nucleus galaxies (SBNGs) studied by Balzano (1983) and to the sample of compact Kiso galaxies studied by Comte et al. (1993). In common with SBNGs, MBGs are galaxies where the burst of star formation is clearly located in the nuclear region (Coziol et al. 1993a, 1994). Related to this star formation activity, these galaxies possess spectra that are identical to H II regions but with a relatively low level of excitation when compared to the so-called H II galaxies (Terlevich et al. 1991). The electron density is higher, on average, than in H II regions found in the discs of galaxies. The infrared luminosities and *IRAS* colours both indicate an important dust content more or less related to the star formation activity. The mean metallicity of the MBGs is near-solar, suggesting that they are relatively evolved galaxies (this differs from H II galaxies; see Masegosa, Moles & Campos-Aguilar 1994).

An intriguing characteristic concerns the morphological distribution of the MBGs: while they are found among all types of galaxies, they are more common among early-type spirals. This morphological preference has already been observed by Balzano (1983) for the Markarian SBNGs. No interpretation has yet been given for this particular distribution. Another question that is still debatable is the origin of the star-forming activity in starbursts. While it is generally

* Brazilian CNPq fellow; E-mail: clarissa@if.ufrgs.br.

believed that some kind of interaction is responsible for the enhancement of the star formation rate (SFR) in these objects, evidence for the origin of this phenomenon is not recognizable in all cases (Campos-Aguilar & Moles 1991; Coziol, Barth & Demers 1993b).

In order to establish the nature of the activity of the MBGs more accurately, and to try to discover something about its origin, we began a follow-up imaging programme of our candidates. Our first sample of MBGs consists of 15 candidates with available spectrophotometric data. Because no additional selection criterion was applied, this sample should be typical of the MBGs.

In this paper, our goals are to explore structures related to bursts of star formation in SBNGs and to provide a quantitative description of the morphological aspects of these objects. Our analysis is based on techniques previously utilized by other authors to study normal galaxies (Nieto et al. 1992; Prieto et al. 1992a,b), allowing direct comparison with our galaxies. In particular, we will look for quantitative evidence supporting the hypothesis of past interaction in SBNGs and try to distinguish what is the role of interaction and bars in this phenomenon. In a future paper (Barth, Coziol & Demers 1995, in preparation), the same kind of analysis will be performed on a sample of AGNs to explore possible differences between the star formation processes occurring in those galaxies and in SBNGs.

1.1 Basic morphological components of galaxies

It is well known that spiral galaxies generally present two basic components: a bulge and a disc. Currently, several theories and models associate these components with different evolutionary stages of the formation of the galaxy (Sandage 1986). From the observational point of view, the luminosity profile of the galaxy may be used to identify and isolate the different components. This is the procedure usually adopted for normal spiral galaxy studies, although this kind of separation can be an adequate representation of no more than one-half of the observed spirals (Boronson 1981; Kent 1986, 1987). In fact, separation of the profiles is frequently very difficult, because of the presence of an intermediate zone found in many galaxies (Talbot, Jensen & Dufour 1979; Prieto et al. 1992b). In the luminosity profile, this zone does not follow an $R^{1/4}$ (where R is the galactocentric distance) bulge + exponential disc luminosity law. The first interpretation put forward to explain this phenomenon was the presence of a third component of intermediate morphology, a lenticular thick disc distribution (Freeman 1977). This thick disc was considered as having been formed during an intermediate evolutionary stage of the galaxy. Subsequent studies tend to associate this intermediate zone with processes of vigorous star formation (Boronson 1981). The increased luminosity caused by this enhanced star formation would lead to remarkable departures from the simple two-component radial luminosity profile. According to Prieto et al. (1992b), this zone can be well modelled by a combination of young stars in arms embedded in dust, without requiring a lenticular component in the old disc population. This conclusion is further supported by their observational data, which show that the intermediate region has colours that are bluer than an older stellar population of a hypothetical thick disc. A natural consequence of this last interpretation is that it is very difficult to fit a two-component luminosity profile law in galaxies showing regions of strong star formation.

Generally, it is impossible to isolate only two components of the luminosity profile in starburst nucleus galaxies, because there are, in several cases, well-defined intermediate regions of vigorous star formation. Furthermore, in our observations, other structures, such as bars and rings, were detected, which also cannot be fitted by a simple two-component model. This particular situation requires the use of more sophisticated techniques to gain information on the morphologies of the MBG starbursts. For example, the analysis of the elliptical parameters of the galaxy isophotal shapes should yield interesting information.

1.2 Fitting of elliptical isophotes and isophotal shapes

The method of fitting elliptical isophotes on the observed isophotal levels of the galaxies by interactive adjustment of the elliptical parameters is the best way to reproduce their shape. With this procedure, we obtain a surface brightness profile that represents the average along each elliptical isophote. This mean radial profile has an improved signal-to-noise ratio, as compared with a single profile taken along the major axis of the galaxy. Using this technique, we can access some structures of the object, such as bars, arms and regions of star formation or dust, which modulate the radial luminosity profile. Another important profile, also obtained by this procedure, is the colour index profile. The comparison of the different colour profiles along the galaxy allows us to identify regions of star formation and dust absorption, and the redder bulge population. Additional parameters used are the variation of ellipticities (eps), the position angles of major axes (PA), and the measure of deviation from pure elliptical features of the isophotes (high harmonics a_4 and b_4). Each of them provides important information on the morphology. Essentially, all of these parameters are closely related to physical properties and dynamical features and, consequently, to evolutionary stages of the galaxies.

Position angle curves with strong variations can reflect true inhomogeneous mass distributions (Zaritsky & Lo 1986). Such deviations from asymmetry can lead to non-circular motions of the gas, increasing the rate of collisions, as well as the radial transport of gas towards the galactic centre. It has been suggested by Scoville & Hersh (1979) that this could be a mechanism for enhancing the density of gas in the nucleus and for triggering star formation there. Furthermore, when compared in more than one filter, the variation of the PA indicates the presence of dust patches. The strongest deviations from the elliptical form are observed in galaxies with dust absorption and strong tidal interactions. Indeed, the highest values of isophotal twists are measured in interacting galaxies. This suggests that most of the twists are produced by close encounters or mergers (Di Tulio 1979; Kormendy 1982; Bender & Möllenhoff 1987).

The deviations from pure elliptical features of the isophotes are quantified by the use of the so-called a_4 coefficient, normalized to the semimajor axis of the ellipse a. It is obtained by expanding the radial deviations in the Fourier

series (see, e.g., Bender & Möllenhoff 1987):

$$\delta r_j = \sum_{i=1}^{N} a_i \cos\left(\frac{2\pi ij}{N}\right) + b_i \sin\left(\frac{2\pi ij}{N}\right)$$

where δr_j is the radial deviation of an isophote from a pure ellipse on the sample point j, and a_i and b_i are the Fourier coefficients. The behaviour of the parameter a_4 determines the character of the isophotes: boxy ($a_4 < 0$) or pointed ($a_4 > 0$). A non-zero value of b_4 means that the deviation from the pure ellipse of the isophote is not aligned with its semimajor axis. These characters (boxy and pointed) are not a question of projection of the galaxy onto the sky, but are related to intrinsic properties of the object (such as optical, radio and X-ray emission; Bender et al. 1989). Pointed isophotes are associated with the presence of a disc, superimposed onto a spheroidal distribution. Boxy isophotes are not well understood, but there is observational and theoretical evidence (Binney & Petrou 1985; May, van Albada & Norman 1985; Bender 1988; Nieto & Bender 1989) that they can be caused by interactions. Also, results by Bender et al. (1989) and Nieto & Bender (1989) suggest that boxy and discy ellipticals represent different lines of galaxy evolution.

We present the observations and reduction procedures, as well as the data, in Section 2. The results are in Section 3. The discussion and conclusions are presented in Section 4.

2 OBSERVATIONS

2.1 Data acquisition

The imaging observations discussed in this paper were carried out during four nights in 1992 September and one night in 1993 September, at the $f/8$ focus of the 1.6-m telescope of the Mont Mégantic Observatory. All the images were obtained during photometric dark time. The imaging was made with a Thompson 1024×1024 CCD, using standard Johnson *BVRI* filters. The angular pixel size is 0.31 arcsec^2, which gives a field of 5.3×5.3 arcmin^2. The seeing conditions were of the order of 2 arcsec. Each night, one standard photometric field (NGC 7790), from Christian et al. (1985), was observed to calibrate the images. For each galaxy, we took three images in each filter, with exposure times of 900 s for B, 600 s for V and 200 s for R and I.

2.2 Reduction and calibration

The data were reduced using the IRAF packages, applying standard procedures. Bad lines and columns at the edges were cut, resulting in an effective frame of 4.1 arcmin. For each frame, field stars and background galaxies were removed and replaced by interpolation to sky level values. Sky subtraction was carried out for each image, measuring the median of the sky level counts in several regions of the frames, well beyond the galaxy image.

The instrumental magnitudes of standard stars were measured to obtain the transformation equations for each filter. For the calibration, we followed the same procedure as Grondin et al. (1990). Correction for atmospheric extinction was carried out using standard coefficients for each band. The integration time used allowed us to obtain images with fainter isophotes of about 24 to 25 mag arcsec^{-2} in B, 24 mag arcsec^{-2} in V, 23 mag arcsec^{-2} in R and 22 mag arcsec^{-2} in I filters. Because of the generally peculiar morphologies of the galaxies of our sample, total magnitudes of the galaxies were obtained from CCD synthetic aperture photometry. We fitted standard growth curves to the CCD photometry, integrated within circular apertures over the sky-subtracted images, and measured the total asymptotic magnitude in each band.

2.3 Analytical methodology

The fitting procedure was carried out using the IRAF package STSDAS.ISOPHOTE.ELLIPSE. The analysis was based on the azimuthally averaged luminosity profiles, and the behaviour of the elliptical parameters. These profiles and parameters for each galaxy are presented in Figs 1–3. The ellipticity, position angle and the higher-order harmonics of the Fourier series expansion of the fitted ellipses are inferred as functions of the semimajor axis a. Harmonics a_4 and b_4 are given as percentages of the semimajor axis, as is usual. The position angles are measured from east, anticlockwise. The geometrical parameters presented are taken beyond the seeing radius of each image; that is, parameters within the seeing radius are not even plotted in Figs 1–3.

In order to identify regions of star formation, we have analysed colour profiles (azimuthally averaged, as well as taken over the two axes directions) and colour maps (the calibrated $B-I$ image) for each galaxy. They give two types of information: when the image is red we can infer that the population is redder (older or with higher metallicity) than in the bluer areas, or that the starlight is partially obscured by dust. It is possible to distinguish between the two effects qualitatively. Prieto et al. (1992a,b) successfully used this kind of analysis. Their criterion was that 'reddening plus decreased surface brightness is probably due to dust, reddening plus increased surface brightness is almost certainly a stellar [population] effect'. By simultaneous inspection of the luminosity profiles, colour and PA of the ellipses, we can infer where the $B-I$ curve has a bluer or a redder excess in relation to the underlying radial gradient. On the colour maps, dust absorption can also be identified by its patchy appearance.

The geometrical parameters given by the fitting can be either colour-independent or not. Generally, a parameter's dependence on colour is usually interpreted as resulting from absorption effects. It arises from the differential absorption in each observed wavelength. In this sense, for *BVRI* imaging, the filter I is the least affected by dust absorption. Therefore, dust lanes can also be detected by comparison of parameters on different filters. In Figs 1–3 we present the parameters (ellipticities, position angles and higher-order harmonics a_4 and b_4) derived from I-band isophotes, when they are wavelength-independent. Otherwise, we show either V or I isophotal parameters, for comparison. Absorption leads to different position angles for each band, and generally to rounder isophotes in short-wave light bands. On the other hand, when the isophotes are more elongated in bluer bands, it is probably due to the enhancement of blueness caused by star-forming regions (at the end of bars, for example).

In order to investigate the results, we have defined three regions for each galaxy: the inner, intermediate and outer

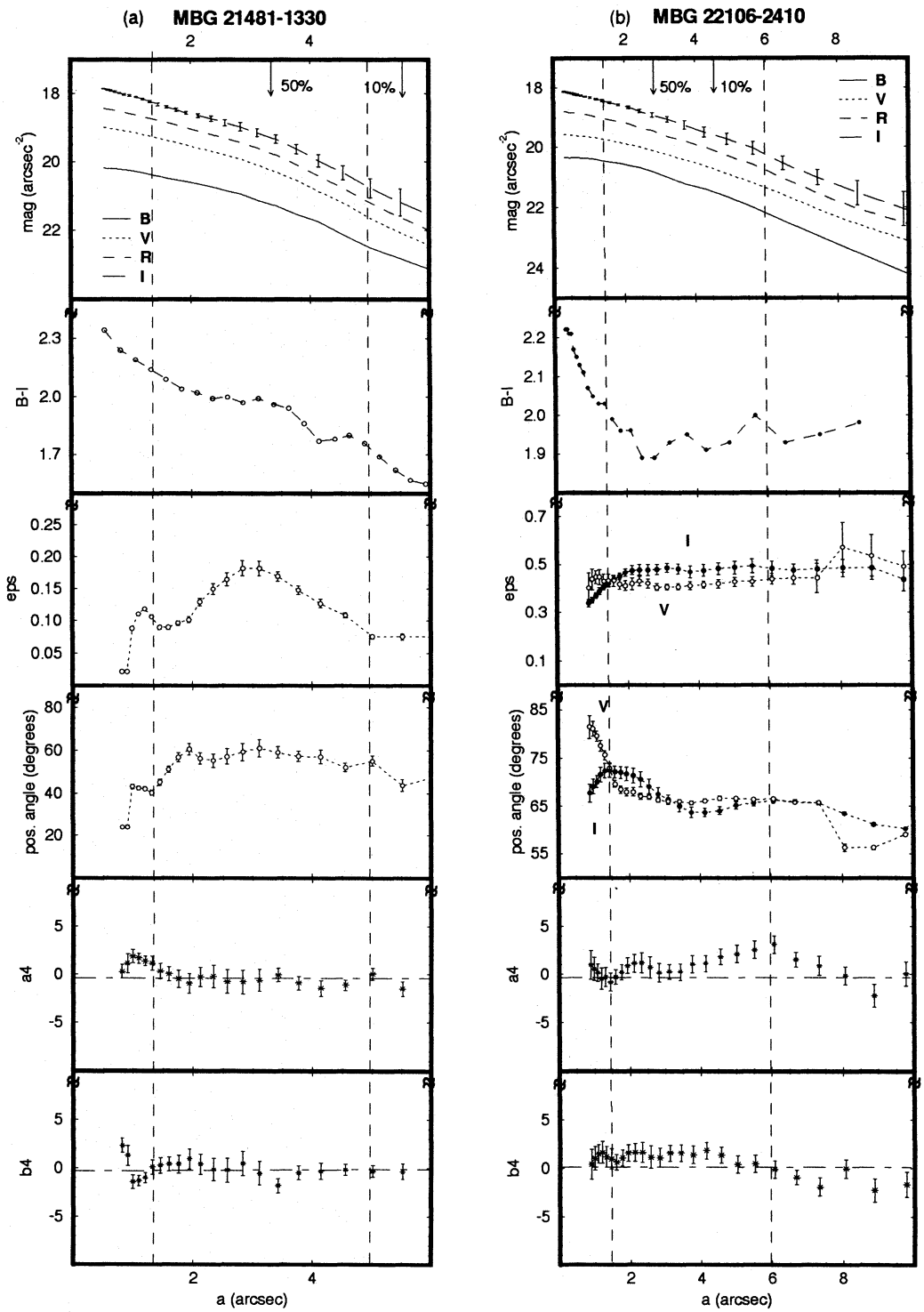

Figure 1. Surface brightness, colour index and geometrical parameters (ellipticities, position angles and harmonics a_4 and b_4) as a function of the semimajor axis length a, for galaxies with extended starbursts. (a) MBG 21481 − 1330; (b) MBG 22106 − 2410; (c) MBG 22537 − 1650.

regions. They are marked in Figs 1–3 by dashed vertical lines. The limit of the inner region was defined as the distance at which the variations of the elliptical parameters are correlated, that is, the distance at which the 'geometrical decoupling' occurs. We will discuss the geometrical decoupling in more detail in the next section. The transition between the inner and outer regions occurs in the intermediate region, where bars and circumnuclear regions are located. The outer regions include external envelopes or discs.

3 RESULTS

3.1 Photometry

We present, in Table 1, the total magnitudes in each filter for the galaxies of our sample. The errors on the measured

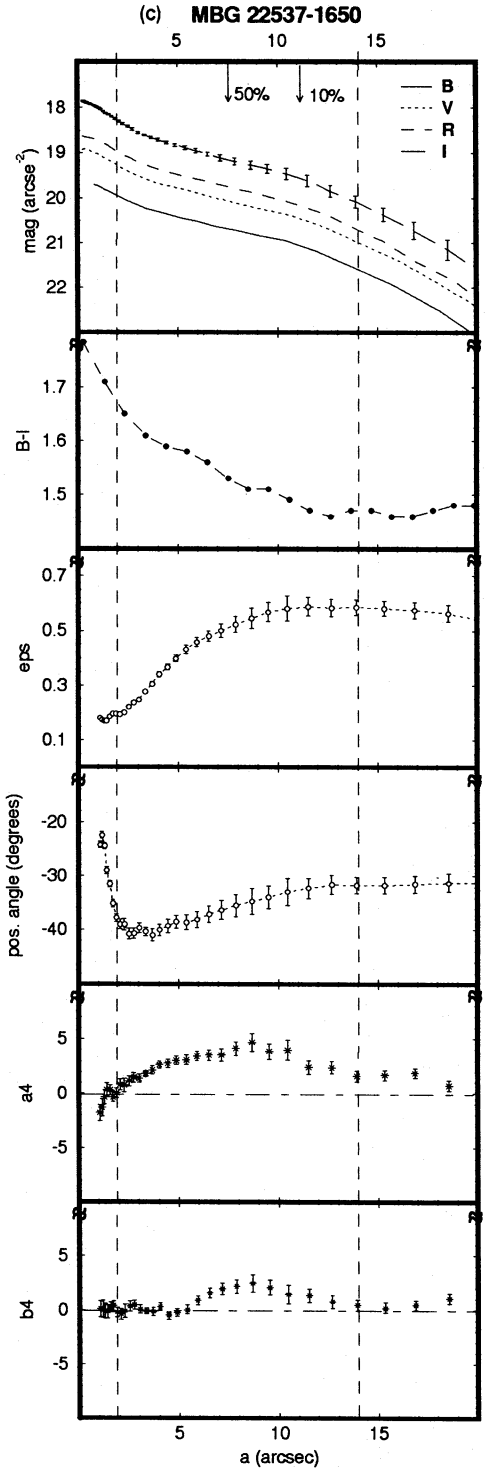

Figure 1 – *continued*

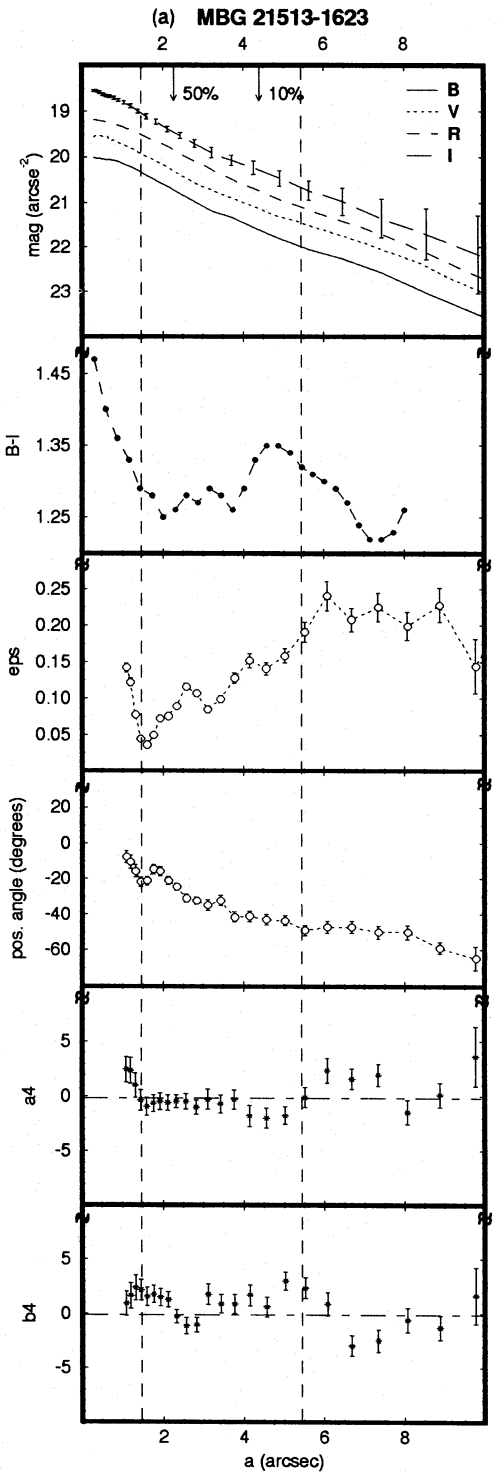

Figure 2. As Fig. 1, for galaxies with circumnuclear regions of star formation. (a) MBG 21513−1623; (b) MBG 22012−1550; (c) MBG 23369−2241; (d) MBG 23382−2047; (e) MBG 00317−2142; (f) MBG 01166−1719; (g) MBG 02072−1022.

magnitudes are mainly due to the calibration procedure, and are evaluated to be ±0.10 mag in *B*, ±0.05 mag in *V* and *R*, and ±0.07 mag in *I*. The relatively large errors on the magnitude reflect the small number of standard stars (~10 each night) used to determine the coefficients of the calibration curve. Because we did not get a good image in *B* of MBG 03353−2439, we use the photometric data published in the NASA/IPAC extragalactic database (NED) for this particular galaxy and filter. Only two other galaxies of our sample have some published aperture photometry. Those data are unfortunately unsuitable for comparison, being either in a different photometric system or of poor quality.

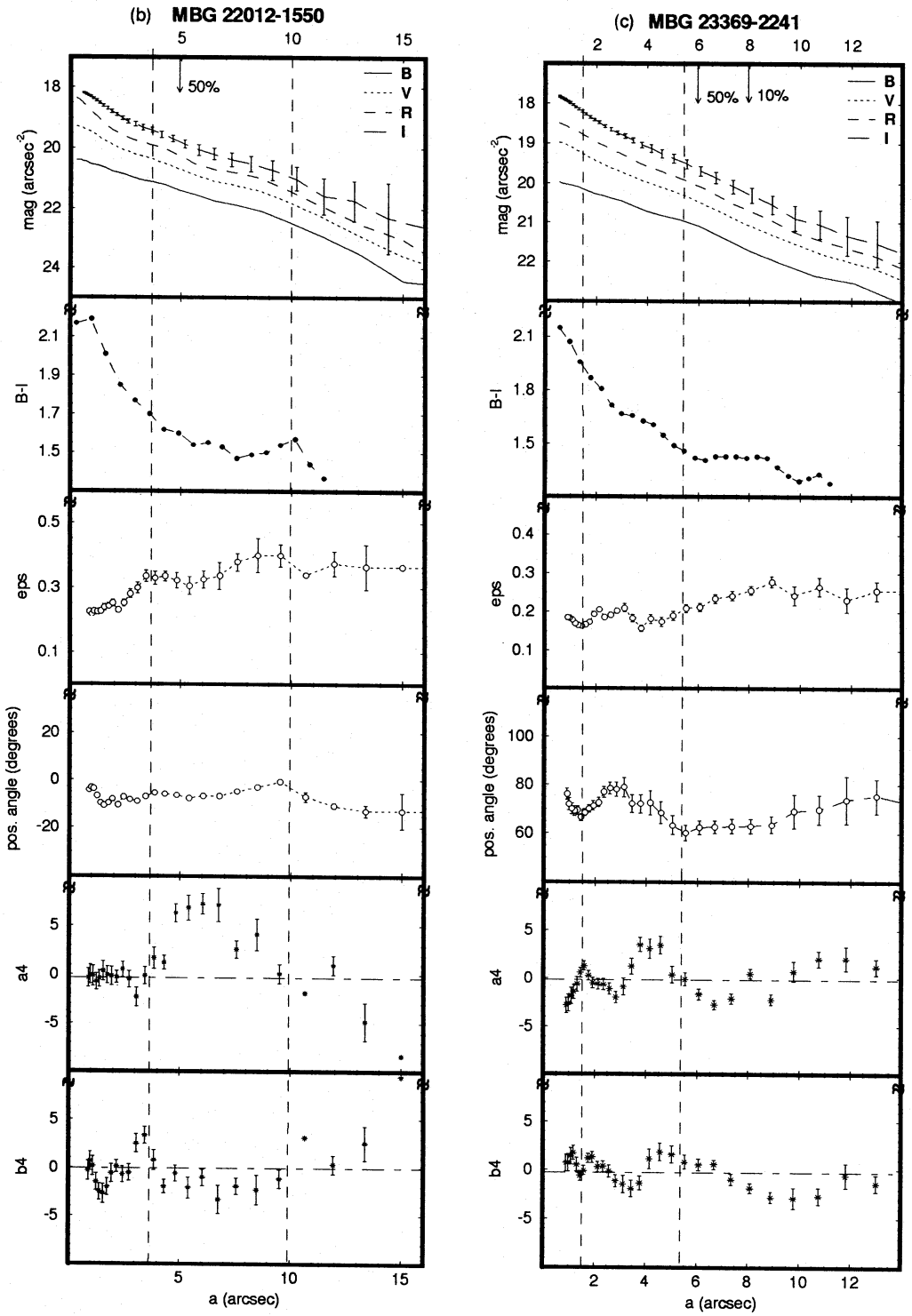

Figure 2 – *continued*

3.2 Morphology

From our images, we can classify the 15 galaxies analysed here in three different general classes. This classification is similar to the one employed recently by Heisler & Vader (1994) for their imaging of a sample of 60-μm peakers. Galaxies of class A (Fig. 4) are the amorphous galaxies (four galaxies). By definition, an amorphous galaxy has a smooth and symmetric light distribution. Except for MBG 02072 – 1022 (Figs 4g and h), which is a member of a loose group, all the galaxies of this class are apparently isolated field galaxies. Class P (Fig. 5) regroups the peculiar galaxies. We define as 'peculiar' any galaxy with various peculiar features: tail (e.g. Fig. 5k), plumes (Figs 5a and c), multiple nucleus (Fig. 5i), bridge (Fig. 5g), or simply a disturbed morphology (Fig. 5e). Six out of 15 of our galaxies are in

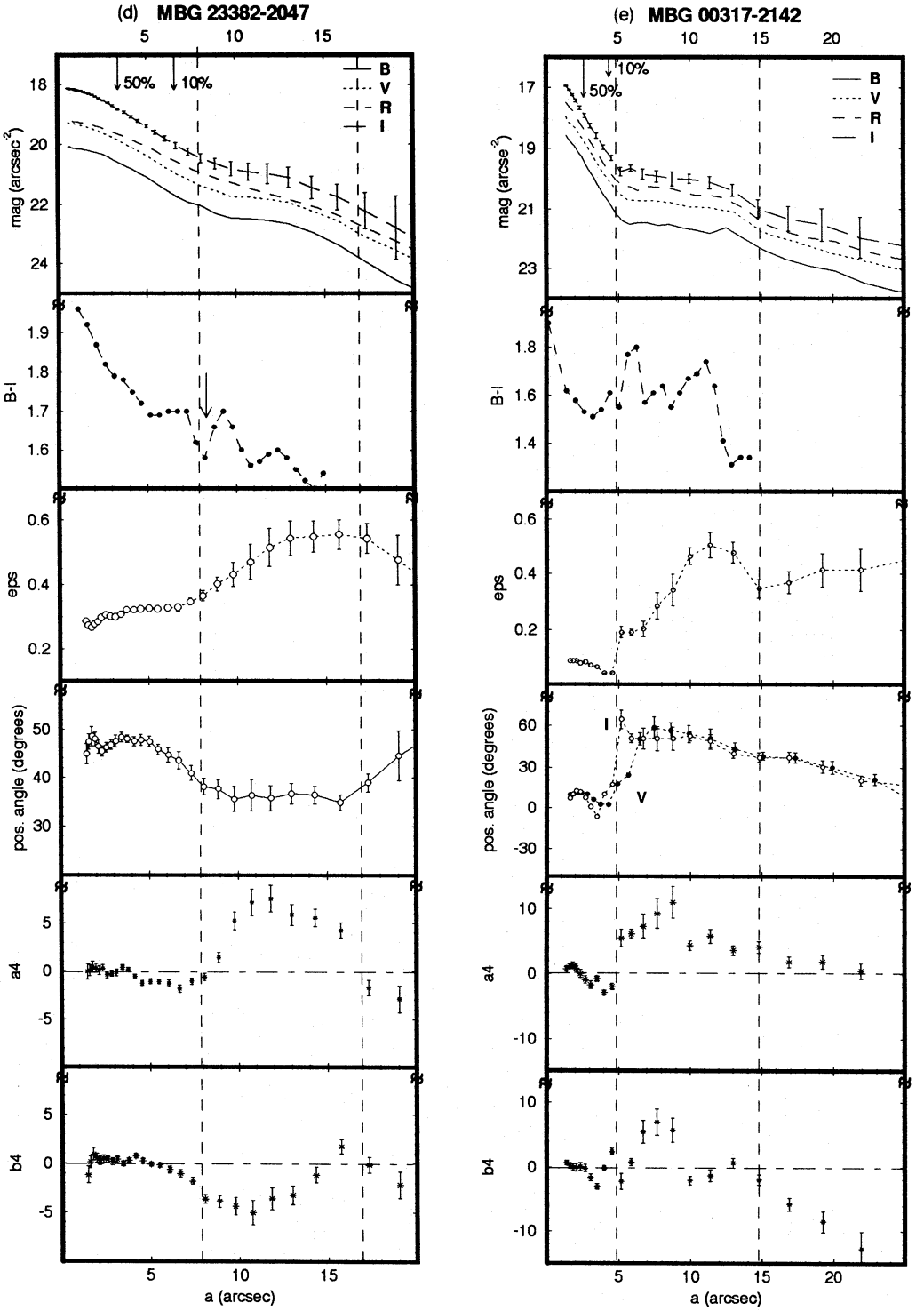

Figure 2 – *continued*

class P. This class contains clear cases of interacting galaxies: either interaction between galaxies of the same size, such as MBG 21513−1623 (Figs 5a and b), or the possible accretion of smaller companions, which is the case for MBG 00461−1259 (Figs 5i and j), and probably for the remaining peculiar galaxies. Finally, class S (Fig. 6) regroups the spiral galaxies (five galaxies). Any galaxy with traces of spiral features will be put into this class. Note that, while the spiral-like structure is evident in the galaxies of this class, they none the less look somewhat peculiar compared with normal spiral galaxies (small, multiple and asymmetrical arms). In particular, they all possess an outer envelope, a feature that is uncommon for normal spirals. This was also observed by Heisler & Vader (1994) for their four spiral galaxies. As remarked by these authors, this particularity is consistent with simulations of self-gravitating discs perturbed by tidal

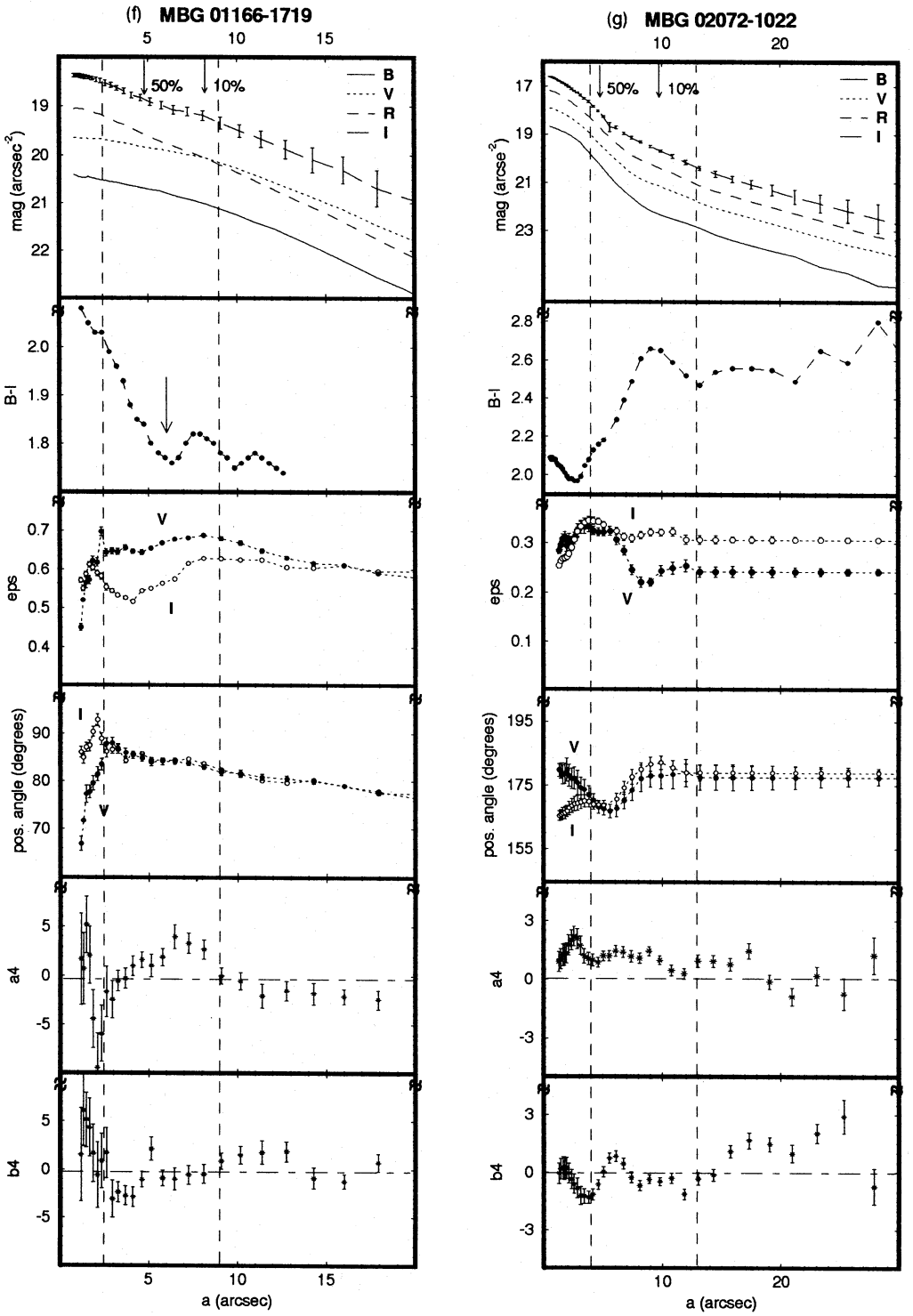

Figure 2 – *continued*

forces of other galaxies. However, only the spiral galaxy MBG 00317−2142 (Figs 6c and d) is a member of a group (Hickson 1982). The four other galaxies of this class are isolated.

3.3 Quantitative analysis

We present a summary of the parameters derived from the isophote fittings in Table 2. Column 2 lists the ellipticities of the external isophotes. Maximum variations of the PA (isophotal twists) for each galaxy are given in column 3. Columns 4 and 5 list the maximum amplitudes of the parameters a_4 and b_4, defined in Section 1.2. In column 6 we indicate the character – boxy (b) or discy (d) – of the isophotes, from the inner to the outer regions. Parentheses indicate uncertain classification. The principal morphological features are listed in column 7. Column 8 gives the spatial characteristics of the extra-nuclear starbursts.

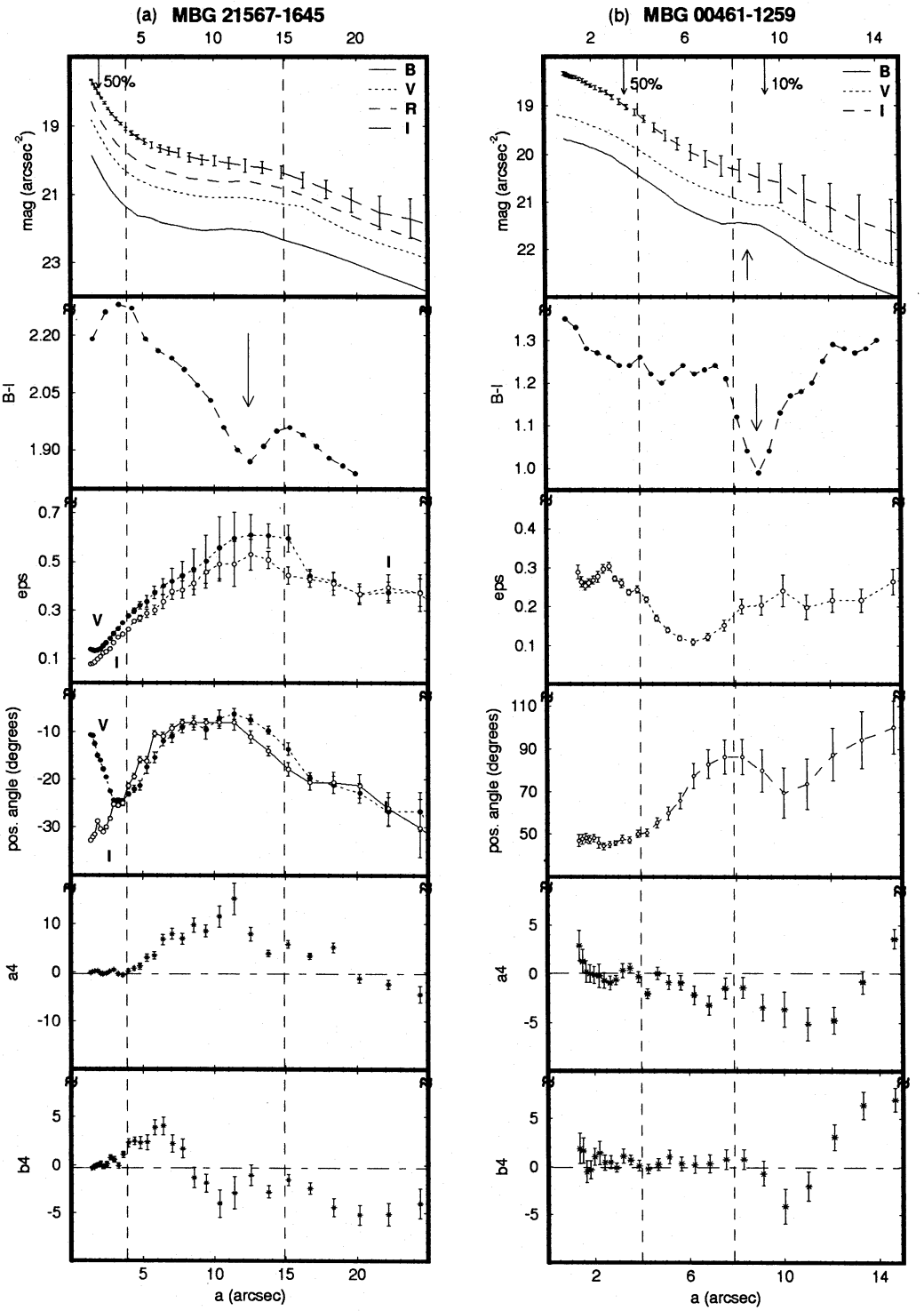

Figure 3. As Fig. 1, for galaxies with hotspots in the disc. (a) MBG 21567 − 1645; (b) MBG 00461 − 1259; (c) MBG 02141 − 1134; (d) MBG 03353 − 2439; (e) MBG 03468 − 2217.

From the point of view of star formation sites, we can distinguish three types of starburst: extended starbursts, intermediate regions of star formation and hotspots in the disc. The extended starbursts correspond well to the amorphous class, with the exception of MBG 02072 − 1022, which we show to be a circumnuclear starburst galaxy, because it presents a decentred starburst. In the 'peculiar' and 'spiral' classes, we find galaxies with intermediate regions and galaxies with hotspots in the disc. All the spirals present a well-defined nucleus in the luminosity profile. A summary of the analysis is given in the following sections.

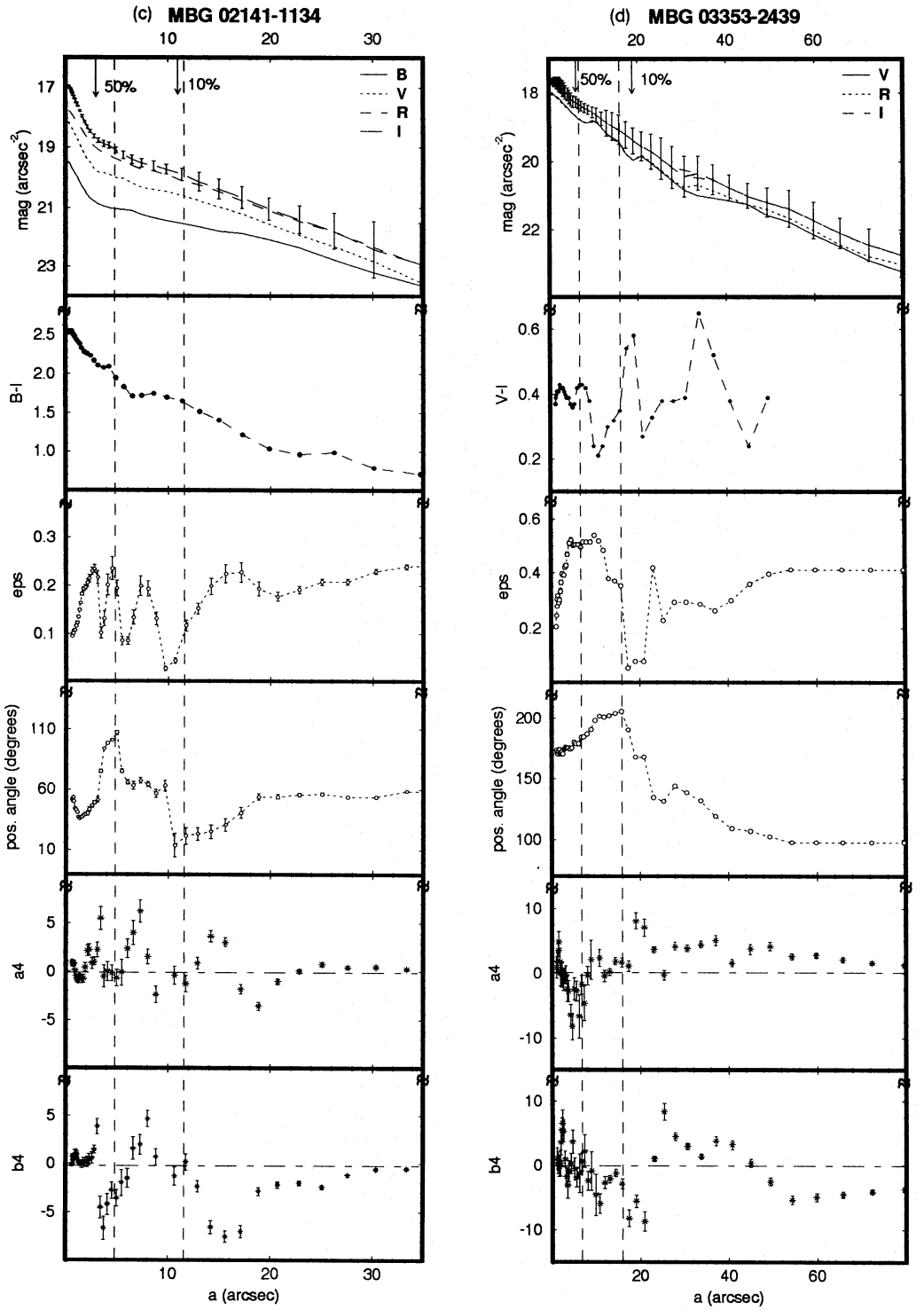

Figure 3 – *continued*

3.3.1 *Galaxies with extended starbursts*

Examples of extended starbursts are MBG 21481 – 1330, 22106 – 2410 and 22537 – 1650. In those galaxies, the Hα emission extends a few kiloparsecs over the central region (see Coziol, Barth & Demers, Paper II). Extended starbursts do not present a clear two-component shape on the surface brightness curves. We do not see a bright central peak, but rather an enlarged bulge in all filters. The $B-I$ colour index varies almost monotonically, from red to blue, with a slightly steeper gradient in the nuclear region of MBG 22537 – 1650 (Fig. 1c). In general, this behaviour corresponds well to the gradient associated with a bulge-dominated system (Prieto et al. 1992b). In the case of MBG 22106 – 2410, both the PA and the ellipticity are colour-dependent, suggesting dust absorption. In MBG 22537 – 1650, the $B-I$ colour image

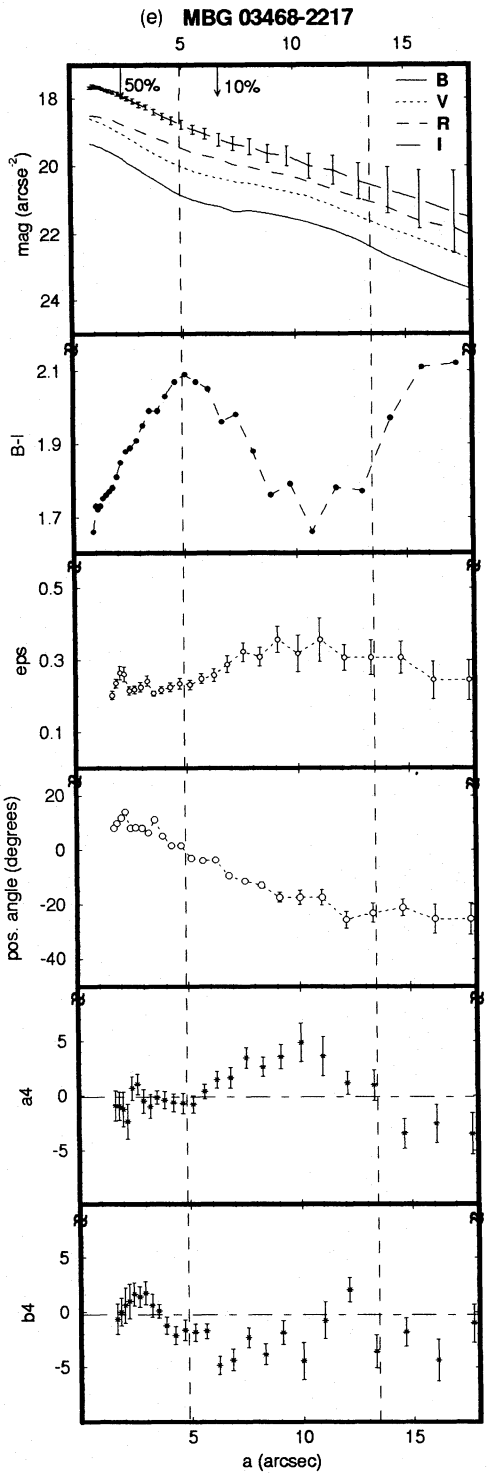

Figure 3 – *continued*

and the colour index profiles taken along the major and minor axes show a different behaviour from the averaged (by the fitting procedure) $B-I$ profile. On the $B-I$ image (Fig. 7a), we see a SE–NW colour gradient, attributed to a dust lane in the galactic plane, which is inclined with respect to the plane of the sky. It implies that the south-eastern side of the galaxy (the bluer side) is its nearer edge. The same effect is noticeable in Fig. 7(b). Howevever, we still see the red bulge superimposed on the $B-I$ colour index profile.

Table 1. Total magnitudes of selected MBGs.

MBG	B_T	V_T	R_T	I_T
21481-1330	16.40	15.28	14.85	14.40
21513-1623	15.77	15.29	14.93	14.62
21567-1645	14.35	13.54	12.98	12.48
22012-1550	15.44	14.61	14.11	13.66
22106-2410	16.32	15.45	14.92	14.40
22537-1650	14.36	13.65	13.34	12.67
23369-2241	14.90	14.19	13.79	13.37
23382-2047	15.22	14.42	14.06	13.49
00317-2142	13.89	13.18	12.76	12.32
00461-1259	14.53	13.92	13.58	13.22
01166-1719	14.20	13.57	13.14	12.69
02070-1022	14.20	13.25	12.55	11.94
02141-1134	13.82	12.71	12.16	11.84
03353-2439	11.50[a]	10.72	10.66	10.31
03468-2217	14.42	13.53	12.96	12.40

[a]Magnitude from NED.

In MBG 21481−1330, the PA varies by 20° at $a=1.5$ arcsec, corresponding to a local minimum of ellipticity and pointed isophotes ($a_4>0$), suggesting a small disc structure close to the nucleus. The parameter a_4 has a small range of variation for $a>2$ arcsec, indicating that the isophotes have almost no departures from a perfect ellipse. In MBG 22106−2410, positive values of a_4 indicate that a discy system dominates in almost the whole galaxy. MBG 22537−1650 also presents positive values of a_4, but in this case the isophote deviations are produced by rudimentary arms sticking out of an elliptical bulge, with maximum amplitudes ($a_4\approx 5$) and misalignments (positive b_4) at $a=9$ arcsec (Fig. 1c). In the contour map (Fig. 4f), we can see these pointed deformations of the isophotes, which are not aligned with their major axis. The PA (Fig. 1c) changes by approximately 10° along the galaxy.

3.3.2 *Galaxies with intermediate regions of star formation*

The galaxies with intermediate regions of star formation are MBG 21513−1623, 22012−1550, 23369−2241, 23382−2047, 00317−2142, 01166−1719 and 02072−1022. With the exception of MBG 00317−2142 and 02072−1022, all these galaxies were classified as 'peculiars'. Both MBG 00317−2142 and 02072−1022 are members of small groups of galaxies, where the probability of interaction is the highest.

These galaxies all show a red nucleus and a blue intermediate region, corresponding either to a false bulge, coinciding with the FWHM of the Hα central emission (marked as a '50%' arrow in Figs 1–3), or to a bar (in the cases of MBG 23382−2047 and 00317−2142). The peculiar nature of the galaxies can be deduced from the numerous asymmetric structures and distortions on the isophote contours. These structures, as well as bars, are evident in the PAs and ellipticity profiles.

In MBG 00317−2142, the bar corresponds to the plateau between 5 and 12 arcsec in the luminosity profiles (Fig. 2e). Along the bar, the PA remains approximately constant. In the bar region, the isophotes are pointed

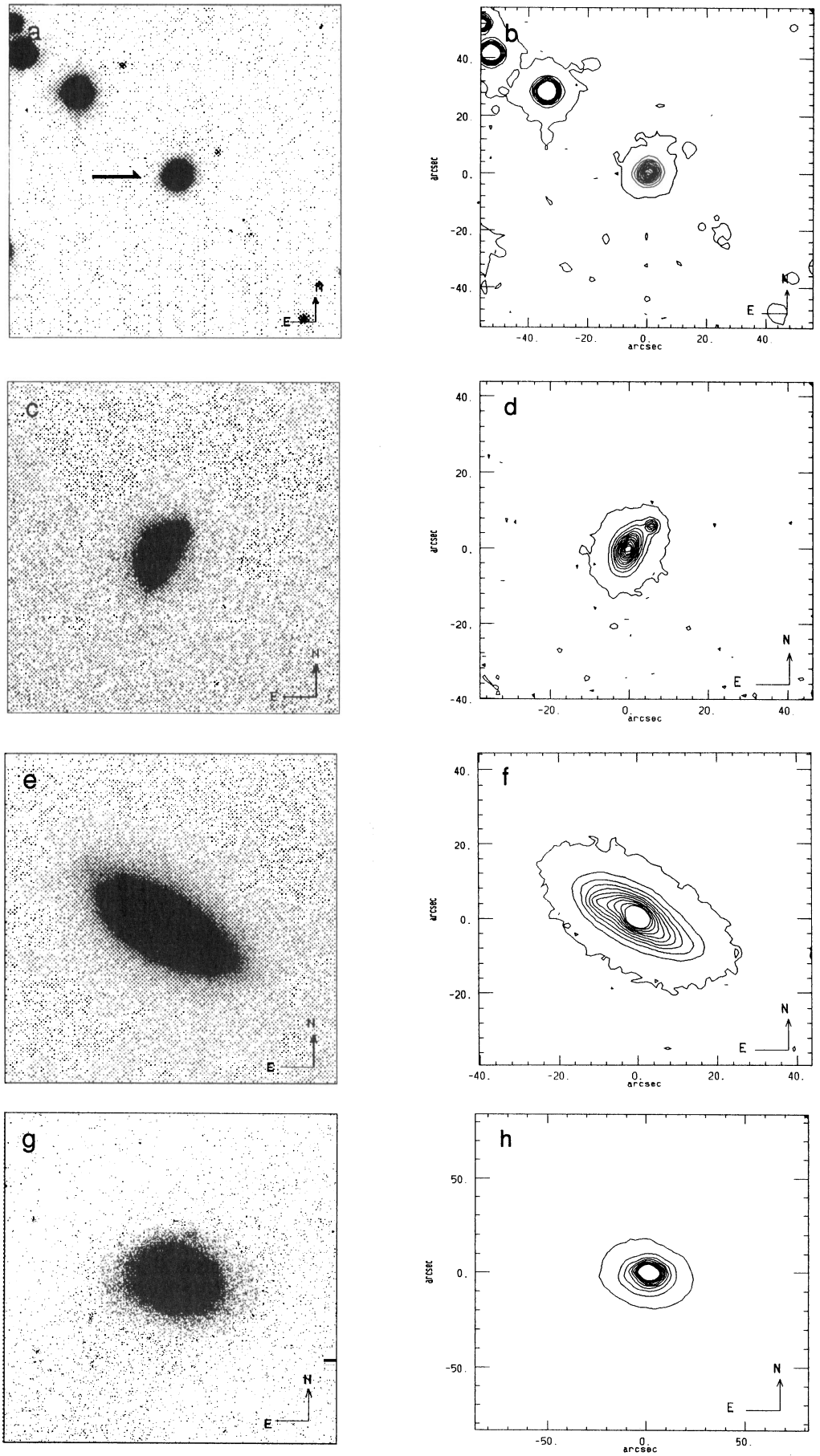

Figure 4. Direct images (left panels) and isophotal contours (right panels) in the V band of galaxies of the 'amorphous' class. For each galaxy, the scales of images and contours are the same. (a) and (b) MBG 21481 − 1330; (c) and (d) MBG 22106 − 2410; (e) and (f) MBG 22537 − 1650; (g) and (h) MBG 02072 − 1022.

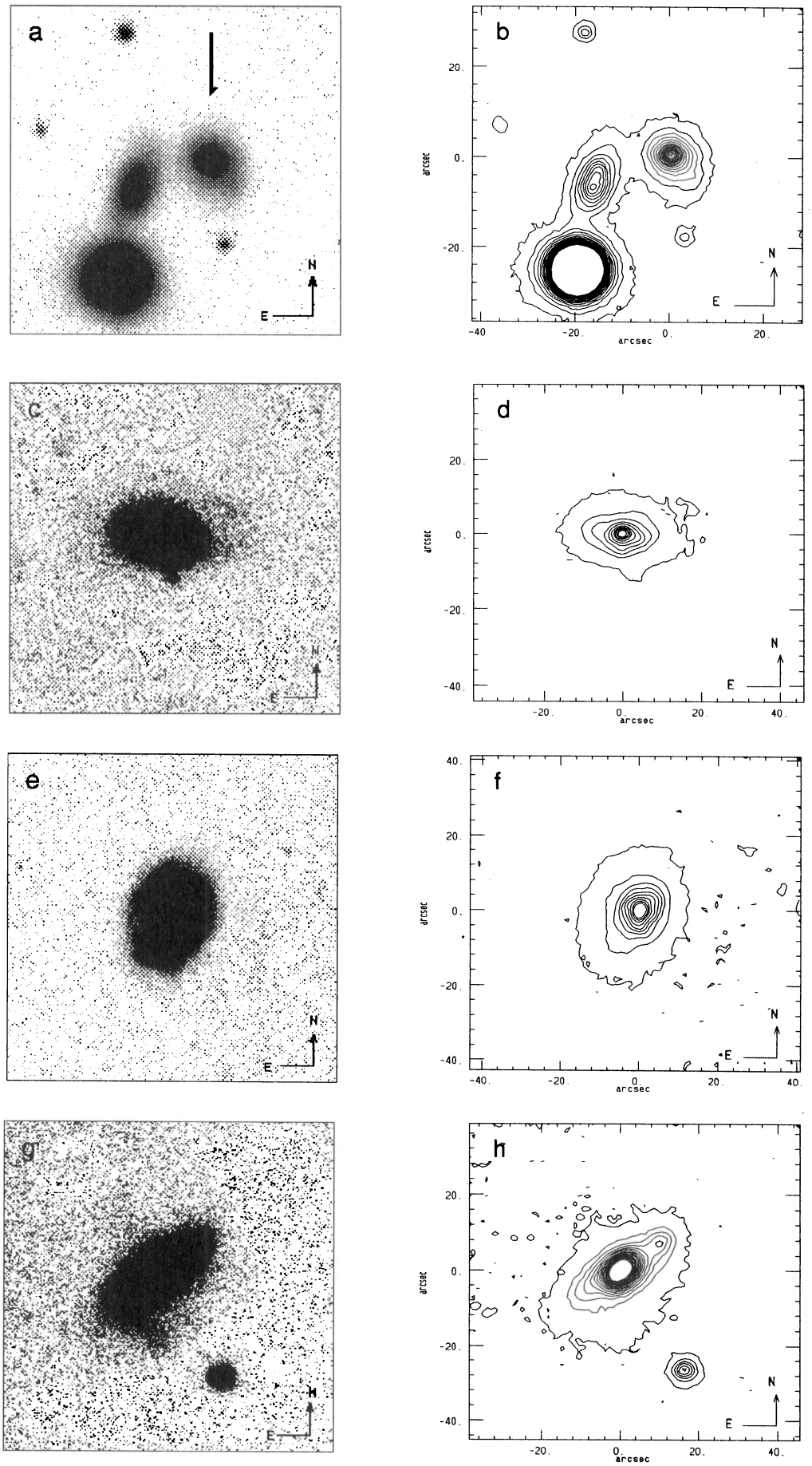

Figure 5. Direct images (left panels) and isophotal contours (right panels) in the V band of galaxies of the 'peculiar' class. For each galaxy, the scales of images and contours are the same. (a) and (b) MBG 21513 − 1623; (c) and (d) MBG 22012 − 1550; (e) and (f) MBG 23369 − 2241; (g) and (h) MBG 23382 − 2047; (i) and (j) MBG 00461 − 1259; (k) and (l) MBG 01166 − 1719.

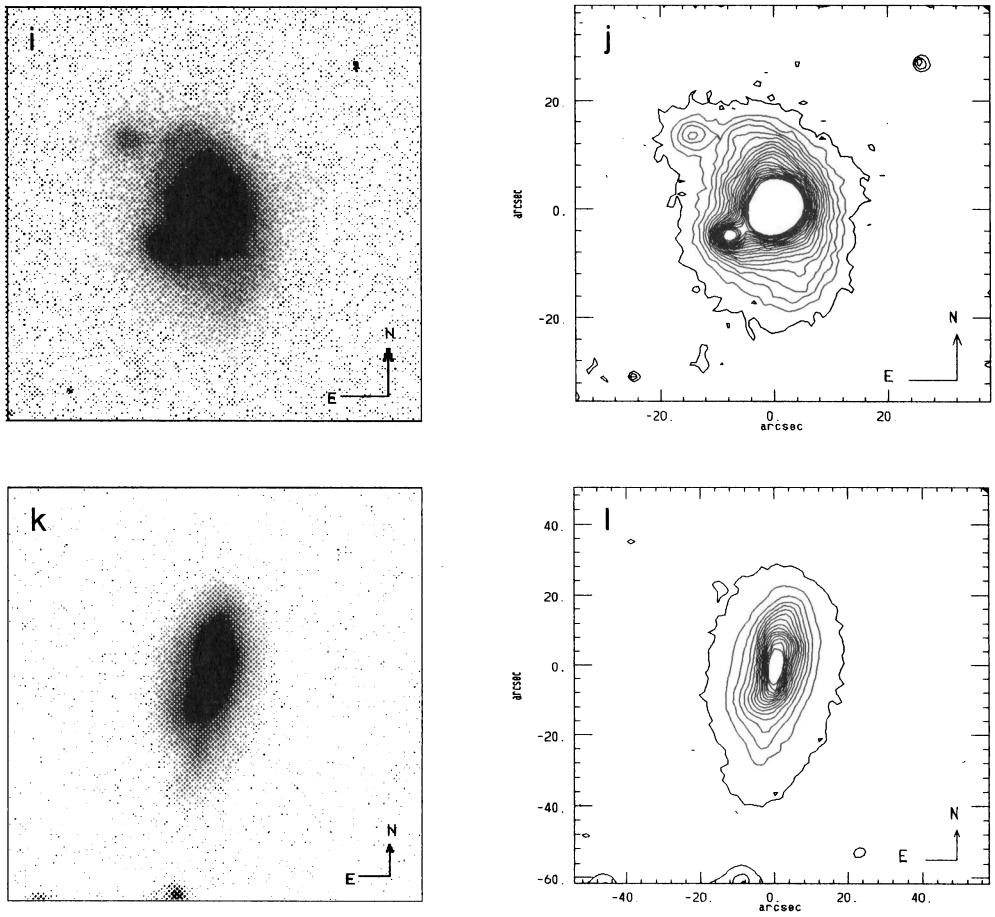

Figure 5 – *continued*

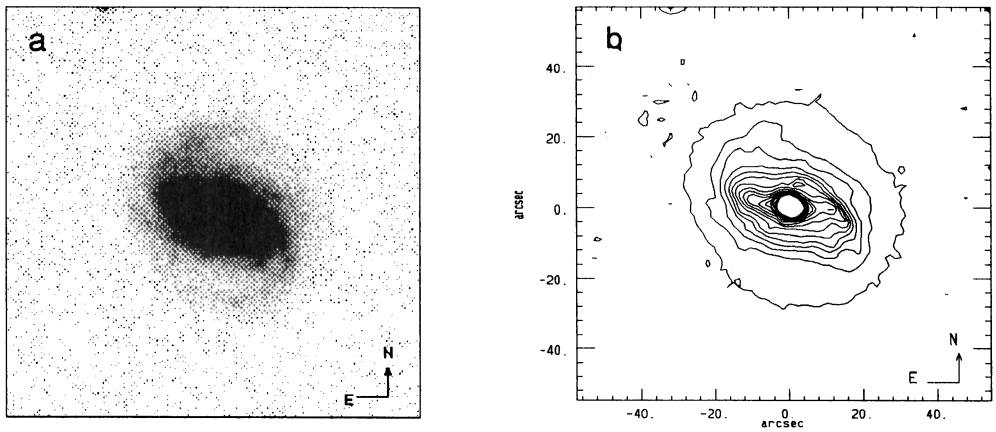

Figure 6. Direct images (left panels) and isophotal contours (right panels) in the V band of galaxies of the 'spiral' class. For each galaxy, the scales of images and contours are the same. (a) and (b) MBG 21567 – 1645; (c) and (d) MBG 00317 – 2142; (e) and (f) MBG 02141 – 1134; (g) and (h) MBG 03353 – 2439; (i) and (j) MBG 03468 – 2217.

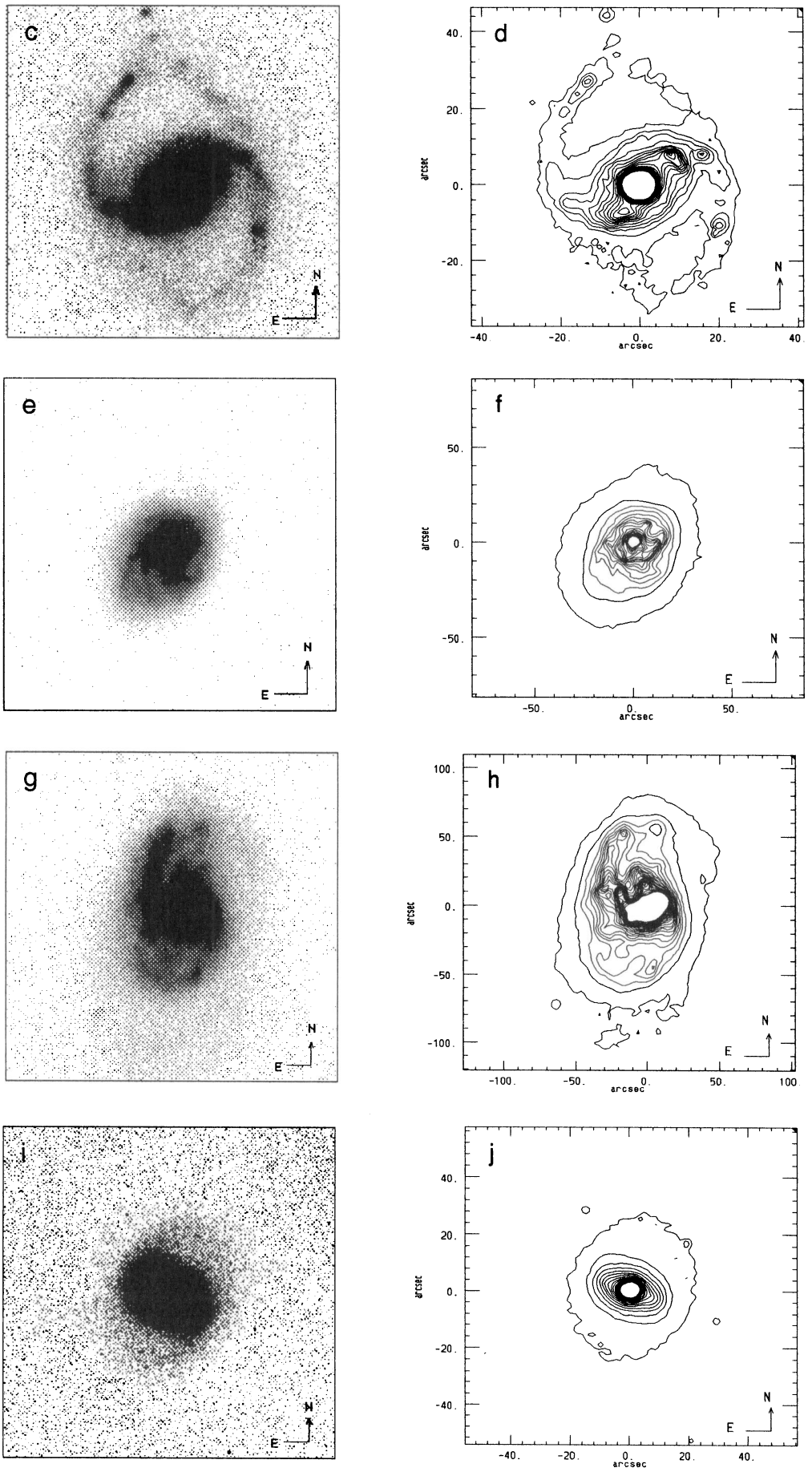

Figure 6 – *continued*

Table 2. Morphological parameters of selected MBGs.

MBG	*eps*	ΔPA	a_4	b_4	deviation of ellipse	morphology	starburst
21481-1330	0.05	-18	-3.5	-10.0	db	compact	extended
21513-1623	0.22	-56	2.0	-3.0	db	compact	circumn.
21567-1645	0.40	+23, -27	15.0	-4.0	db	bar	bar end
22012-1550	0.36	+10, -12	-8.0	9.0	bdb	ring	circumn.
22106-2410	0.48	-9	±3.0	±2.0	d	double nucleus?	extended
22537-1650	0.55	-20,+10	5.0	2.5	d	arms?	extended
23369-2241	0.25	+9, -19, +15	3.5	±2.0	bdb	knots	circumn.
23382-2047	0.51	-13, +10	8.0	-5.0	bdb	bar	circumn+bar end
00317-2142	0.35	-19, +71, -44	11.0	7.0	bdb	bar, late	circumn+bar end
00461-1259	0.22	+41, -17, +30	-5.0	-4.5	dbb	double nucleus	hotspot
01166-1719	0.61	-12	-5.0	-3.0	bdb	bar	circumn.
02072-1022	0.31	+13	-4.0	3.0	d	early pec.	descentered
02141-1134	0.10	+60, -80, +40	4.0	-5.0	d(b)d	double nucleus	hotspots
03353-2439	0.30	+35, -110	±9.0	±9.0	bdd	bar, late pec.	hotspots
03468-2217	0.26	-37[a]	5.0	-5.0	bdb	bar	bar end

[a]Smooth variation over the semimajor axis.

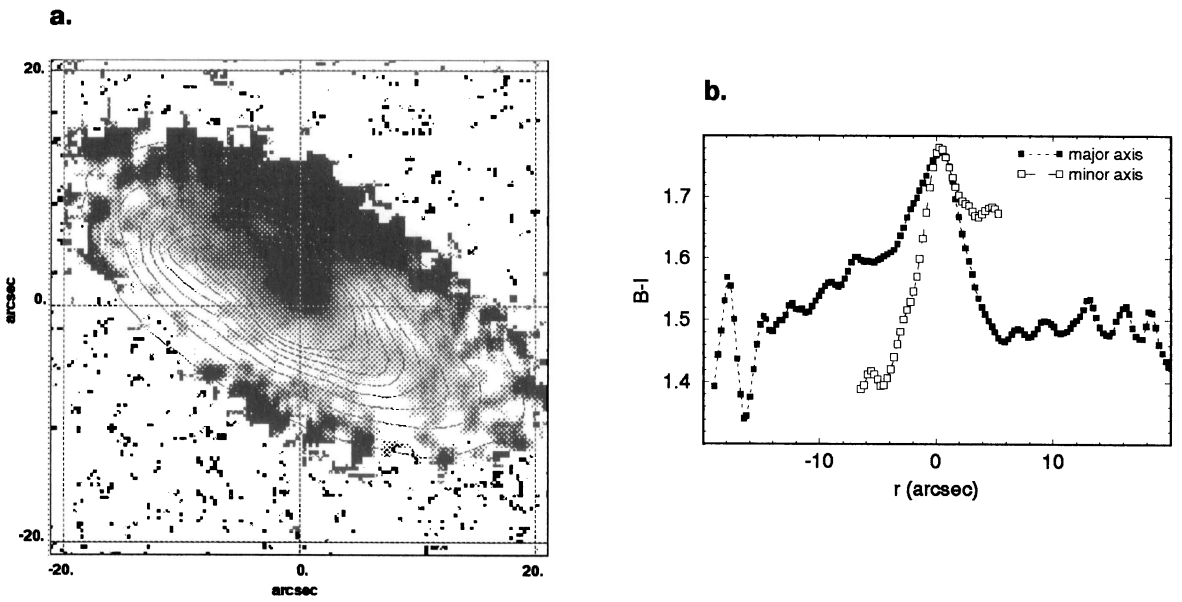

Figure 7. (a) $B-I$ colour image of MBG 22537 − 1650. North is up, east to the left. Dark shades correspond to red features and lighter shades to bluer areas. The contour of the galaxy on filter I is superimposed. Notice the SE–NW colour gradient. (b) $B-I$ colour index profile of MBG 22537 − 1650 in the major and minor axis directions. Arrows indicate blue regions at the north and south sides of the nucleus.

($a_4 \gg 0$), and strongly misaligned with the major axis of the ellipse ($b_4 \gg 0$). It corresponds to regions of star formation located at the end of the bar. Blue features in this region can be inferred by the $B-I$ colour image (Fig. 8a). Inspection of this image also reveals a blue circumnuclear ring, corresponding to the edge of the nuclear starburst (radius 2.7 arcsec or 0.72 kpc; see Paper II). In the colour profiles taken along the directions of the semimajor and semiminor axes (Fig. 8b), we identified the blue ring at $r = \pm 3$ arcsec. We can also see that the reddening is more pronounced in the major axis than in the minor axis direction. The red features along the bar are probably due to dust absorption (fading B), whereas those at the nucleus are probably due to a red bulge population (enhancing R luminosity, see Fig. 2e).

In the galaxy MBG 02072 − 1022, the averaged $B-I$ colour index profile does not describe well the azimuthal variation of the colour index. In the same profile, taken in the major and minor axis directions (Fig. 9b), we see that the galaxy has a red maximum at $r = -4.5$ arcsec and a blue maximum at $r = 4$ arcsec. On the colour map (Fig. 9a), we can visualize the geometry of the $B-I$ distribution. A blue region is clearly seen in the north-west (NW) (lighter spot).

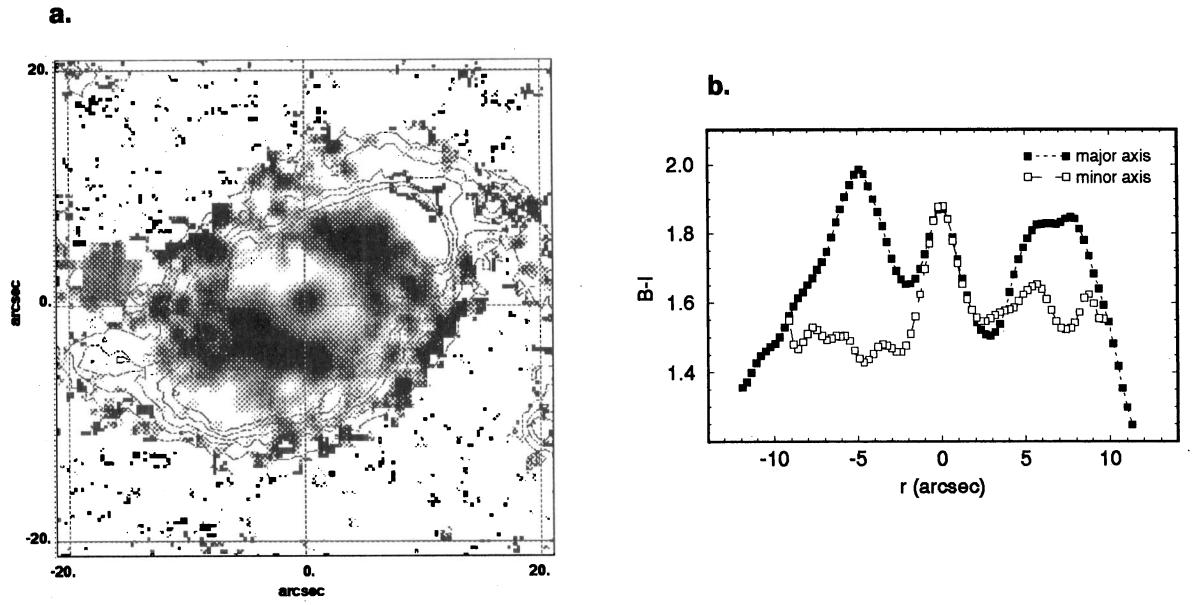

Figure 8. (a) $B-I$ colour image of MBG 00317 − 2142. The orientation and contrast are the same as Fig. 7. The contour of the galaxy on filter I is superimposed. Notice the circumnuclear blue ring. (b) $B-I$ colour index profile of MBG 00317 − 2142 in the major and minor axis directions.

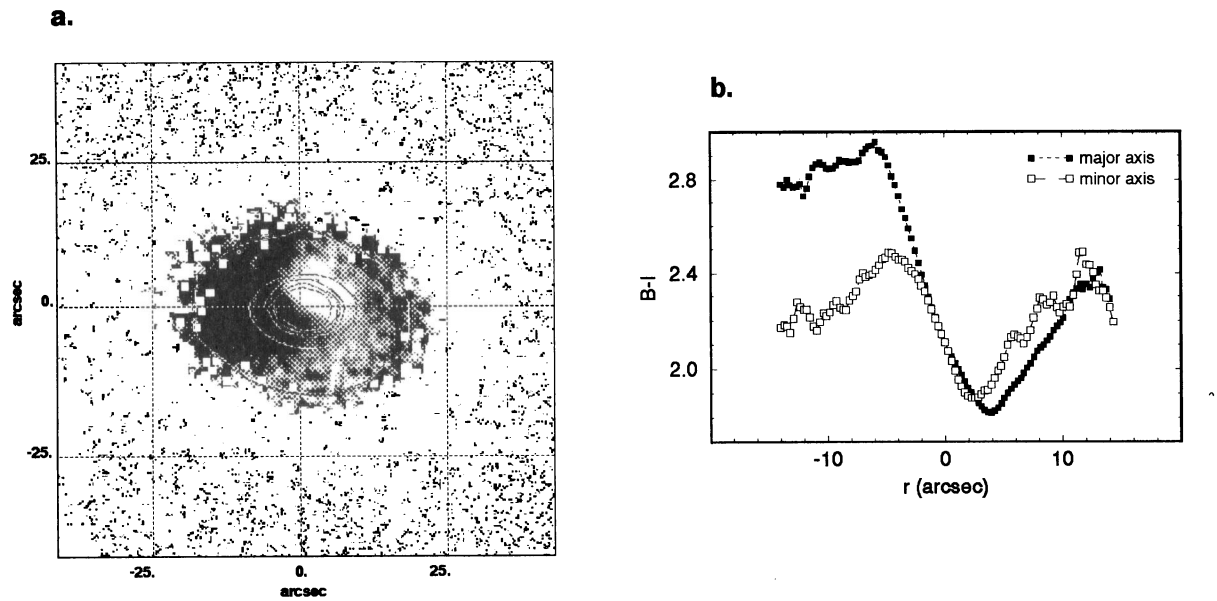

Figure 9. (a) $B-I$ colour image of MBG 02072 − 1022. The orientation and contrast are the same as Fig. 7. (b) $B-I$ colour index profile of MBG 02072 − 1022 in the major and minor axis directions.

The redder region is on the SE side of the nucleus (darker shade) and it is probably caused by dust absorption, which is suggested by the patchy appearance and the different values of the PA in the filters I and V, up to $a=5$ arcsec. The ellipticity is also colour-dependent: differential absorption causes isophotes that are rounder in V than in I, for $a>10$ arcsec.

An interesting point is that this object presents the most spatially asymmetrical nuclear emission of our sample. In Fig. 10 we can see the correspondence between the emission features and the colour map, for the central 20 arcsec. The isophotal contours of the $B-I$ colour image are shown in the lower panel. In the upper panel, we present the isophotal contours of the spectrum (Coziol 1994), over the emission of Hα λ6563, [N II] λ6548 and [N II] λ6583 lines. The maximum emission corresponds well to the peaks of the continuum and the B band. On the eastern side, the emission extends over the bluer region of the colour map. The region obscured by dust (R) does not present emission lines. Consequently, there are no star-forming regions hidden by absorp-

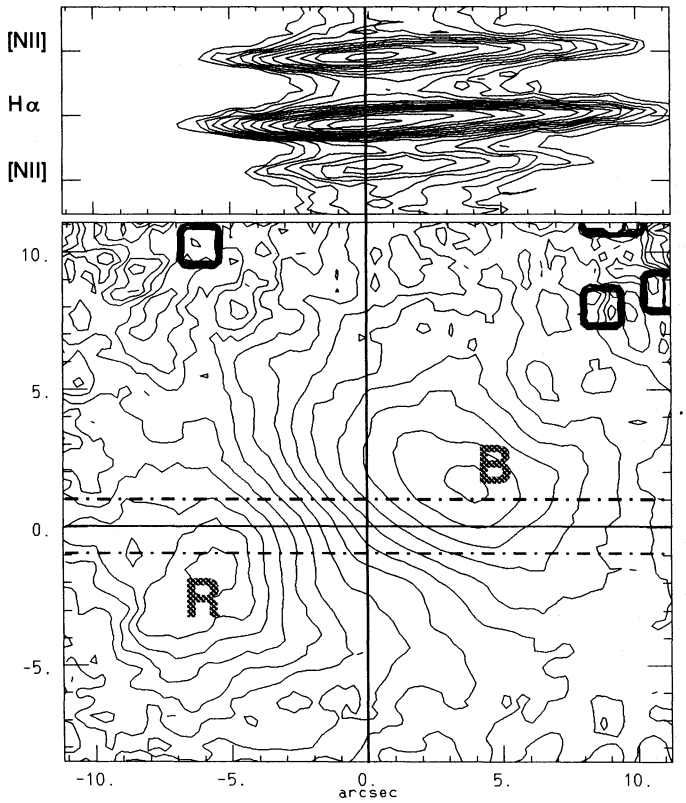

Figure 10. Lower panel: $B-I$ isophotal contour. The blue and red maxima are identified by 'B' and 'R'. The bluest isophote has $B-I=1$ mag arcsec^{-2} and the reddest has $B-I=3$ mag arcsec^{-2}. Dashed lines indicate the region covered by the spectroscopy. The origin of coordinates is at the nucleus, i.e. the peak in B image. Upper panel: isophotal contour, on a logarithmic scale, of the emission Hα λ6563, [N II] λ6548 and [N II] λ6583 lines. Spatial dispersion is on the horizontal axis, with the same scale as the contour map. Wavelength dispersion is on the vertical axis.

tion on the west side of the nucleus. We can see that the bluest region of the colour map does not correspond to the nuclear starburst (i.e. with the peak of the emission lines), but to a circumnuclear region. We interpret this as being an effect of the red bulge population, which decreases the colour contribution with distance from the nucleus.

In general, we observe a variation of the a_4 parameter as we move outwards from discy isophotes to boxy isophotes, reflecting the dominance of the bulge. One exception is MBG 00317 – 2142, with outer discy isophotes ($a_4 \approx 2$), indicating that the disc dominates outside.

3.3.3 *Galaxies with hotspots on the disc*

Examples of galaxies with hotspots on the disc are MBG 21567 – 1645, 00461 – 1259, 02141 – 1134, 03353 – 2439 and 03468 – 2217. With the exception of MBG 00461 – 1259, all these galaxies were classified as spirals. In these galaxies, we do not see the false bulge effect. The hotspots correspond either to starbursts located at the end of a bar or to numerous active star-forming regions in different peculiar arms. In MBG 00461 – 1259, one of the hotspots is in fact a second nucleus. This galaxy shows the bluest central colour index of our sample ($B-I \approx 1.35$ mag arcsec^{-2}). It is an obvious case of a merger of two galaxies.

In MBG 03468 – 2217, the nucleus is more peaked in the B filter than in the I filter (in Fig. 3e, the region with $a<5$ arcsec), thus producing a blue gradient of the $B-I$ index profile towards the centre of the galaxy. If we look at the colour profiles taken on the major and minor axes (Fig. 11b), we see the same behaviour: the nucleus is bluer than its surrounding regions in both directions. This gradient is opposite to those of the other nuclei of our sample. By comparison with the colours of the other nuclei, we see that the nucleus of MBG 03468 – 2217 is not bluer than the rest of the sample. In this case, the circumnuclear region shows

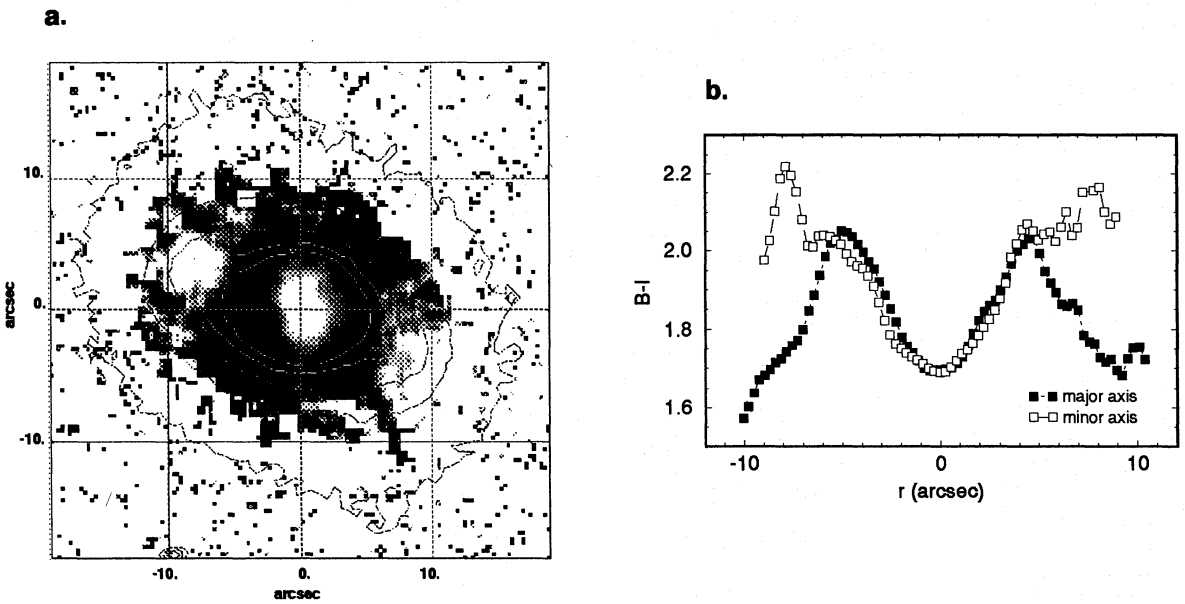

Figure 11. (a) $B-I$ colour image of MBG 03468 – 2217. The orientation and contrast are the same as the other images. (b) $B-I$ colour index profile of MBG 03468 – 2217 in the major and minor axis directions.

redder colours than the other circumnuclear regions analysed in this study.

With the exception of MBG 03353−2439, all these galaxies show boxy isophotes outwards, reflecting the bulge-dominating system.

4 DISCUSSION

4.1 General considerations

The circumnuclear regions and extended starbursts inferred by the colour profiles of all the galaxies in this study match well the extended Hα emission observed spectroscopically. The dimension of these extended regions are of the order of a few kiloparsecs (median value of 1.6 kpc), similar to those seen by Phillips et al. (1986). Only for one object (MBG 23369−2241) have we found that the principal activity comes from the circumnuclear region rather than from the nucleus.

It is interesting to note that almost all the objects analysed here have colour gradients from red to blue when moving from the centre outwards. Although it is difficult to determine which is the most important contribution to the reddish colour of the inner region (old population, dust absorption or probably both), we consider that in most of the cases, it is an effect of the prominent bulge of early-type galaxies contaminating the blue colours of the nuclear star-forming regions. We have carefully inspected the colour images and the geometrical parameters in each filter band to determine where the absorption is present as a dominant factor. For example, the galaxy MBG 22106−2410 shows a difference in PA of 20° between its V and I isophotes in the inner region, with eps ≈ 0.4. This difference of orientation, when in elongated isophotes, is very significant and almost certainly due to a differential absorption by dust in the nucleus. In our sample, we have only four galaxies for which we can detect similar absorption in the inner region. For the other galaxies, the geometrical parameters are identical in this particular region.

For the barred galaxies, the brightness of the bulge deforms the bar isophotes. Almost all the bar structures detected in the galaxies of our sample have discy isophotes, while normal galaxies in general present boxy bars. As demonstrated by Athanassoula et al. (1990), the large bulges of early-type galaxies change the elongated bar isophotes into rounder ones, and change their character from boxy to discy, thus producing 'lemon-shaped' isophotes. These authors have masked out bulge pixels, in order to remove the enlarged central part from the bar isophote. In our case, because we deal with nuclear starbursts, the central region isophotes are so extended over the bar that, after the mask procedure, not enough bar pixels remain to obtain a meaningful fit. Therefore, because we have not been able to apply the same technique, the discy character of bars in this sample comes from a superposition of bar + bulge systems, and the values of bar ellipticities we measured ($0.3 < \overline{\text{eps}} < 0.6$) are probably underestimated.

4.2 Role of interaction

A high interaction rate among our galaxies is suggested by the high frequency of dust and isophote twists. From the analysis of the colour maps, averaged $B-I$ profiles and profiles taken over the major and minor axes, we have verified that all the galaxies show several patterns of absorption, such as dust lanes and redder patches. Isophote twists seen on external isophotes are interpreted as the result of interactions (Nieto et al. 1992). Correlations between internal twists and features on the PA profile, the ellipticity profile and the a_4 profile suggest that twists of internal isophotes are due to substructures strongly overlapping each other. The existence of such substructures in the galaxies of our sample is demonstrated by simultaneous analysis of the parameters presented here. For the galaxies of types E and S0, this fact is more interesting, because these objects have more complex structures than pure ellipsoid or single disk + bulge systems.

Nieto et al. (1991) defined 'geometric decoupling' as the existence of a separate central entity distinguished by features in the ellipticity, orientation and a_4 profiles. These authors have found that photometric substructures were coinciding in radius with the kinematic substructures, or 'kinematically decoupled cores' of elliptical galaxies. They suggest that geometrical decoupling may be taken as evidence for the presence of kinematically decoupled cores, since kinematically decoupled cores do show geometric decoupling as well. The inverse is not true: the kinematic decoupling is not always apparent, probably because of unfavourable inclination, surface brightness or velocity distribution. The consequence is that geometric decoupling, similar to kinematical decoupling, can be an indication that a merging or accretion process has taken place. Buson et al. (1993) observed such geometrical decouplings in elliptical and S0 galaxies with extended optical emission lines. Our data show geometric decoupling also. In Figs 1–3, we have identified the radius of geometrical decoupling for each object as the 'inner region' (up to the first dashed line). In general, it is external to the 'core radius' [similar to results obtained by Nieto et al. (1991)]. We have tried to examine how the ionized gas is distributed with respect to the internal substructures. In Figs 1–3 the radii corresponding to the isophote at 50 per cent and at 10 per cent of the Hα flux are indicated. We can see that, for unbarred galaxies, the Hα emission extends beyond the 'decoupling radius', suggesting that the ionized gas and the stellar population have different distributions. For barred galaxies, the ionized gas lies within the 'decoupling radius'. For these objects the 'decoupling radius' is the radius where the bar begins. Our data cannot determine whether or not stellar formation is suppressed inside the bars, because the spectroscopy of these objects is taken in directions which generally are not aligned with the bar axis. Nevertheless, this result indicates that, for the barred galaxies of our sample, the nuclear starburst is spatially more concentrated than it is for unbarred ones.

The occurrence of internal isophotal twists is very high in our sample. In Table 2 we list the measured ΔPA. In order to select the twists that are not due to dust absorption, we list in this table only the variations in PA that are identical in all filters. Several galaxies show more than one twist in their PA profile. For those cases we have, in Table 2, column 3, more than one value of ΔPA. The sign indicates the direction of the variation (anticlockwise variations are positive). The observed isophotal twists in our sample are related to the presence of bars, for SBa and later types, or with geometrical decoupling (and probably kinematical decoupling), for S0

and E galaxies. The strength of the twists suggests inhomogeneous distributions, internal mass transfer or mass accretion by interaction process. The connection of these events with the observed starbursts is highly probable.

The level of boxiness and discyness of our sample is larger than that of normal early-type galaxies, which lies in the range $-1 < a_4 < 2$ (Bender, Döbereiner & Möllenhoff 1988). We can see in Table 2 that the a_4 parameter has maximum amplitudes of -9 to 15. This corresponds well to the variation found by Smith & Hintzen (1991) for interacting galaxies. Thus, besides the isophotal twists, the high values of a_4 also reflect the disturbed morphology of these objects.

The proposed accretion of gas could be verified by further imaging through narrow-band filters and subsequent comparison with the analysis presented here. With this procedure, Buson et al. (1993) have verified that the stellar and gaseous components frequently have misaligned axes of symmetry, suggesting that gas was probably accreted from outside.

The colour index distribution of the MBGs is compatible with the hypothesis of previous interactions. In Fig. 12 we present two colour–colour diagrams, comparing the colours of the MBGs with those of a sample of normal galaxies and a sample of Arp–Madore interacting galaxies (Smith & Hintzen 1991). Our sample has a wider distribution of colours than normal galaxies [it is also a characteristic of Arp galaxies in general; see Larson & Tinsley (1978)].

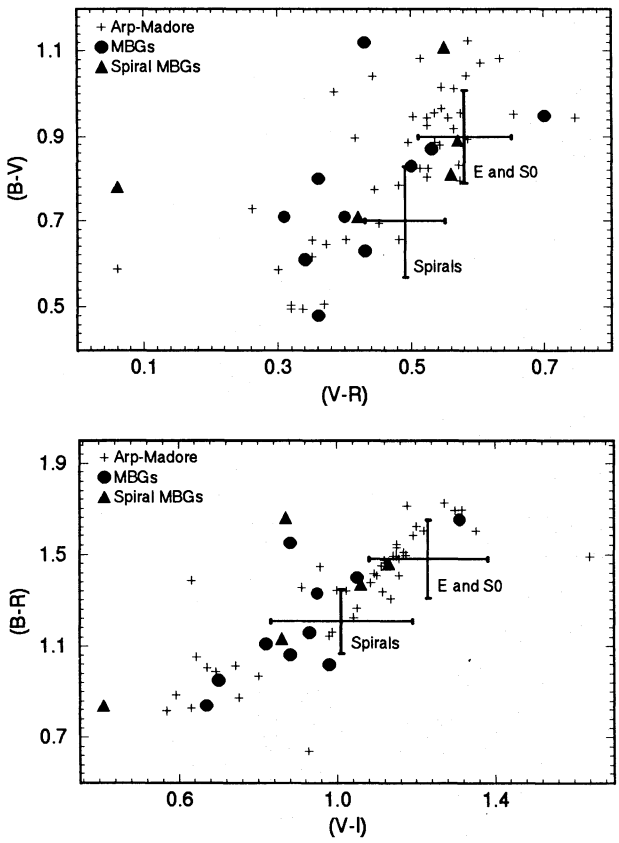

Figure 12. Colour–colour diagrams of MBGs and Arp–Madore galaxies. Mean values and dispersions for spirals and early-type normal galaxies are indicated (38 early-types and 30 spirals, compiled from Smith & Hintzen 1991).

4.3 The relationship between bars and starbursts

Several studies (Arsenault 1989 and references therein) have shown that most starbursts and activie galactic nuclei (AGNs) occur in galaxies with bars and rings. In his work, Arsenault (1989) concluded that star formation is linked to the perturbations of orbits associated with the non-axisymmetrical potential of these structures. He also suggested that one can verify if barred and ringed starburst galaxies have higher luminosities than non-barred and non-ringed ones. For the galaxies in this work, no correlations between B, Hα and IR luminosities and the presence of bars are found. We were interested in verifying, with a larger number of objects, if there is still no correlation between luminosities and the presence of bars. With this purpose in mind, we took all the MBG starbursts for which morphological classification and line fluxes are available, along with the published data from the samples of Stauffer (1982), Balzano (1983) and Keel (1983). We examined the distribution of Hα for barred and unbarred galaxies in the three samples. The mean and median values of the distributions are shown in Table 3. We can see that these values are not significantly different for barred and unbarred galaxies. We performed a Kolmogorov–Smirnov test for a total of 210 objects. The results are also listed in Table 3. The statistical test shows that the two distributions (barred and unbarred galaxies) are not significantly different.

Another interesting suggestion from Arsenault (1989) is that, for the non-barred starburst galaxies, the non-axisymmetrical potential is provided by interactive events. We found that the galaxies of our sample show evidence of interaction (isophotal asymmetries, peculiar morphologies and close companions). We verified that there is a trend for starbursts in barred and unbarred galaxies to have the same luminosity. This suggests that interactions can cause, as efficiently as bars, non-axisymmetrical potentials that lead to star formation in the inner Lindblad resonances. If we consider a sufficient amount of gas and a non-axisymmetrical potential as being necessary conditions for an enhancement of activity in the nucleus, a bar system naturally provides the second condition but interactions can provide both.

5 CONCLUSIONS

We have presented luminosity profiles and parameters derived from isophote fittings for a sample of 15 selected MBGs. The general colour gradients, from red to blue moving from the centre outwards, are interpreted as an effect of the old population in the prominent bulge superimposed on the nuclear starburst. In a minority of cases, absorption by

Table 3. Parameters of the L(Hα) distribution of barred and unbarred galaxies of the samples of Balzano (1983), Stauffer (1982), Keel (1983) and MBGs.

sample	log L(Hα) mean	log L(Hα) median	Kolmogorov-Smirnov discrepancy	Kolmogorov-Smirnov significance
barred (138 obj.)	6.21±0.08	6.21	0.16	0.1358
unbarred (81 obj.)	6.06±0.10	5.93		

dust can also contribute to the reddening of the central region, especially when dust lanes are seen in the circumnuclear regions.

We observe a high frequency of dust and isophote twists. The level of boxiness and discyness of our sample is larger than that of normal early-type galaxies, reflecting the disturbed morphology of these objects. It is highly probable that these characteristics are connected with the observed starbursts, leading us to suggest a previous history of interactions. Furthermore, the MBGs analysed here have a wide range of colours, similar to Arp–Madore interacting galaxies. Contrary to normal galaxies, colours are not correlated with morphological type. The fact that we did not see merger events 'on the spot' and the absence of visible companions for the majority of the galaxies in this sample suggest that the interactions may have taken place a very long time ago.

Simultaneous analysis of the optical images and long-slit spectroscopy shows that the nuclear starburst is more concentrated for barred galaxies than for unbarred ones. In the case of the latter, the ionized gas covers a larger fraction of their total surface; in some cases, the galaxy is a global starburst. However, starbursts in barred and unbarred galaxies show no differences in terms of Hα and IR total luminosities.

ACKNOWLEDGMENTS

We acknowledge the support of the staff of the Observatoire du Mont Mégantic. We are very grateful to Ivo Busko, for his help concerning the STSDAS packages and for his modifications to the STSDAS.ISOPHOTE.ELLIPSE program. Thanks are due to the anonymous referee for his comments and suggestions, which have helped to improve this paper. CSB thanks the Brazilian Conselho Nacional de Desenvolvimento Científico e Tecnológico–CNPq, for financial support. Financial support from the Natural Sciences and Engineering Research Council of Canada and the Québec FCAR are acknowledged. This research has made use of the NASA/IPAC Extragalactic Database (NED), which is operated by the Jet Propulsion Laboratory, California Institute of Technology, under contract with the National Aeronautics and Space Administration.

REFERENCES

Arsenault R., 1989, A&A, 217, 66
Athanassoula E., Morin S., Wozniak H., Puy D., Pierce M. J., Lombard J., Bosna A., 1990, MNRAS, 245, 130
Balzano V. A., 1983, ApJ, 268, 602
Bender R., 1988, A&A, 202, L5
Bender R., Möllenhoff C., 1987, A&A, 177, 71
Bender R., Döbereiner S., Möllenhoff C., 1988, A&AS, 74, 385
Bender R., Surma P., Döbereiner S., Möllenhoff C., Madjesky R., 1989, A&A, 217, 35
Binney J. J., Petrou M., 1985, MNRAS, 214, 449
Boronson T., 1981, ApJS, 46, 177
Buson L. M. et al., 1993, A&A, 280, 409
Campos-Aguilar A., Moles M., 1991, A&A, 241, 358
Christian C. A., Adams M., Barnes J. V., Butcher H., Hayes D. S., Mould J. R., Siegel M., 1985, PASP, 97, 363
Comte G., Augarde R., Chalabaev A., Kunth D., Maehara H., 1994, A&A, 285, 1
Coziol R., 1994, PhD thesis, Université de Montréal
Coziol R., Demers S., Peña M., Torres-Peimbert S., Fontaine G., Wesemael F., Lamontagne R., 1993a, AJ, 105, 35
Coziol R., Barth C. S., Demers S., 1993b, in Shlosman I., ed., Mass-Transfer-Induced Activity in Galaxies. Cambridge Univ. Press, Cambridge, p. 296.
Coziol R., Demers S., Peña M., Barneoud R., 1994, AJ, 108, 405
Coziol R., Barth C. S., Demers S., 1995, MNRAS, 276, 1245 (Paper II this issue)
Demers S., Kibblewhite E. J., Irwin M. J., Nithakorn D. S., Béland S., Fontaine G., Wesemael F., 1986, AJ, 92, 878
Di Tulio G. A., 1979, A&AS, 37, 591
Freeman K. C., 1977, in Berkhuijsen E. M., Wielebinski R., eds, Proc. IAU Symp. 77, Structure and Properties of Nearby Galaxies. Reidel, Dordrecht, p. 3
Grondin L., Demers S., Kunkel W. E., Irwin M. J., 1990, AJ, 100, 663
Heisler C. A., Vader J. P., 1994, AJ, 107, 35
Hickson P., 1982, ApJ, 255, 382
Keel W. C., 1983, ApJS, 52, 229
Kent S. M., 1986, AJ, 91, 1301
Kent S. M., 1987, AJ, 93, 816
Kormendy J., 1982, in Martinet L., Mayor M., eds, Morphology and Dynamics of Galaxies. Saas Fee, p. 113
Larson R. B., Tinsley B. M., 1978, ApJ, 219, 46
Maehara H., Noguchi T., Takase B., Handa T., 1987, PASJ, 39, 393
Masegosa J., Moles M., Campos-Aguilar A., 1994, ApJ, 420, 576
May A., van Albada T. S., Norman C. A., 1985, MNRAS, 214, 131
Mazzarella J. M., Balzano V. A., 1986, ApJS, 62, 751
Nieto J.-L., Bender R., 1989, A&A, 215, 266
Nieto J.-L., Bender R., Arnaud J., Surma P., 1991, A&A, 244, L25
Nieto J.-L., Bender R., Poulain P., Surma P., 1992, A&A, 257, 97
Phillips M. M., Jenkins C. R., Dopita M. A., Sadler E. M., Binette L., 1986, AJ, 91, 1062
Prieto M., Longley D. P. T., Perez E., Beckman J. E., Varela A. M., Cepa J., 1992a, A&AS, 93, 557
Prieto M., Beckman J. E., Cepa J., Varela A. M., 1992b, A&A, 257, 85
Sandage A., 1986, A&A, 161, 89
Scoville N. Z., Hersh K., 1979, ApJ, 229, 578
Smith E. P., Hintzen P., 1991, AJ, 101, 410
Stauffer J. P., 1982, ApJS, 50, 517
Terlevich R., Melnick J., Masegosa J., Moles M., Copetti M. V. F., 1991, A&AS, 91, 285
Talbot R. J., Jensen E. B., Dufour R. J., 1979, ApJ, 229, 91
Zaritsky D., Lo K. Y., 1986, ApJ, 303, 66